ACS APPLIED MATERIALS & INTERFACES

Letter

www.acsami.org

Fabrication of Single Gold Particle Arrays with Pattern Directed Electrochemical Deposition

Renping Ma,[†] Nan Lu,[†,*] Lingxiao Liu,[†] Yandong Wang,[†] Shoulei Shi,[†] and Lifeng Chi[†,‡]

[†]State Key Laboratory of Supramolecular Structure and Materials, College of Chemistry, Jilin University, Changchun 130012, P. R. China

[‡]Physikalisches Institut and Center for Nanotechnology (C198eNTech), Westfälische Wilhelms-Universität Münster, D-48149 Münster, Germany

Supporting Information

ABSTRACT: A simple and efficient method for fabricating gold nanoparticle (AuNP) arrays is developed. With this method, the AuNP arrays are fabricated by taking an electrochemical deposition (ECD) process on the ITO substrate, which is initially patterned with nanoimprint lithography (NIL). The stamp for NIL is fabricated by the cost-efficient nanosphere lithography (NSL). The size of the AuNPs can be adjusted by varying the potential and duration of ECD. In this work, the diameters of AuNPs are varied from 130 to 420 nm. The AuNP arrays can be readily extended to other conductive substrates, which may be applied for detecting and sensing.

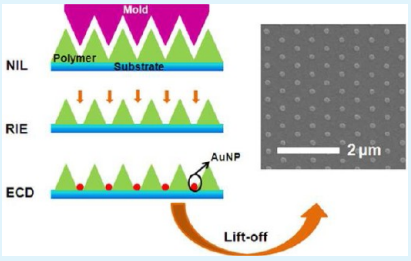

KEYWORDS: *nanoimprint lithography, electrochemical deposition, gold nanoparticle array, nanosphere lithography, template-assisted method*

INTRODUCTION

Metal nanoparticle (NP) arrays have attracted much attention recently because of their wide applications in the fields of sensing,[1−3] catalysis,[4] data storage,[5] as well as etching mask to fabricate periodic semiconductor nanowires[6−8] and templates for the growth of large arrays of aligned carbon nanotubes[9] and ZnO nanorods[10,11] that have been broadly explored in fabricating field-emission displays[12] and ultraviolet nanolasers.[13] The applications depend on the geometry of the NPs and their spatial arrangement. Metal NP arrays can be fabricated by various methods, generally, which can be sorted into two catalogs: direct writing methods and template-assisted methods. The conventional direct writing methods, such as electron-beam lithography (EBL)[14,15] and scanning probe lithography (SPL)[16] can be used for producing arbitrarily shaped particles with various sizes, however, the throughput limits their applications in mass production. The idea of template-assisted approaches is to make the NPs selectively grow or self−assembly[17−19] on the substrates bearing patterns. Block copolymers (BCPs),[20−22] anodized alumina templates (AAO),[23,24] and monolayer or double-layer colloidal crystals in the NSL[10,11,25] have been demonstrated to be templates in producing metallic nanodot arrays. Metal NP arrays are fabricated on predefined patterns through self-assembly,[17,18] evaporation, ECD,[26−28] electroless deposition,[21,29] et al. Among these methods ECD has attracted great attention due to facial controllability of shape and size of NPs under proper deposition conditions and no need for further processing steps. Therefore, the combination of easy control, high throughput, and low cost is still a key issue in creating metal NP arrays in the scale of submicro to nanometer, which is the basic of applications of the particle arrays.

In our previous work, an approach was developed to fabricate arrays of AgNPs on predefined areas by means of ECD combined with NIL.[26] Herein, the mold for NIL we used was derived out of NSL[30−32] because of its low cost and facile controllability of mold periodicity comparing to the well-known self-assembly processes such as AAO[33,34] and BCP.[29,35] AuNPs can be generated directly on the substrate with template-assisted ECD. The particle diameter can be easily controlled by adjusting the potential and duration of ECD using the same stamp. In this work, the AuNPs with the diameters ranging from 130 to 420 nm were fabricated. Furthermore, this method may have potential applications in fabricating AuNP arrays with different periodicities by applying PS spheres with different sizes and the conductive substrate allows applications in the electrochemical fields.

EXPERIMENTAL SECTION

Materials. ITO (10 Ω/sq) was obtained from Jingbo Glass and Display Company, Shenzhen, China. Chloroform, ethanol, and acetone, used for cleaning the substances and the lift-off process, were purchased from Beijing Chemical works at the highest available purity and used without further purification. $HAuCl_4{\cdot}4H_2O$ (AR grade) was from Shanghai Chemical Reagent Co., Ltd. Mr-I 7030E (Micro Resist Technology GmbH, Germany) was used as resist polymer for thermal NIL.

Received: June 19, 2012
Accepted: August 2, 2012
Published: August 2, 2012

   dx.doi.org/10.1021/am3010972 | ACS Appl. Mater. Interfaces 2012, 4, 3779−3783

Fabrication of Stamp. The silicon stamp of nanopillar array was fabricated by NSL as described in our previous study.[36] Reactive-ion etching (RIE) was carried out on a Plasmalab Oxford 80 plus (ICP 65) system (Oxford Instrument Co., UK). The processing gases were SF_6 (25 sccm), CHF_3 (28 sccm) and O_2 (8 sccm), the RF power was 100 W, and the chamber pressure was 30 mTorr. The etching duration was 11 min. Prior to imprinting, the stamp was treated with an antiadhensive layer (tridecafluoro-1, 1, 2, 2-tetrahydrooctyl-trichlorosilane) by the vapor phase deposition, resulting in a very low surface energy. This treatment can prevent the resist polymer from sticking to the stamp during the imprinting process, facilitating the separation of the stamp and the imprinted patterns.

Substrate Patterning. ITO substrates (2×2 cm^2 slices) were sonicated consecutively in the bath of acetone, chloroform, ethanol, and water (Millipore, resistance of 18.2 MΩ · cm) for 5 min, respectively. A 250 nm Mr-I 7030E layer was spin-coated onto the clean ITO substrate, followed by annealing at 90 °C for 5 min to remove residual solvent. The imprinting was carried out on a 2.5-in. Nanoimprinter (Obducat AB, Malmö, Sweden). NIL process was performed at 130 °C, under 40 bar for 500 s. After peeling off the stamp from the substrate at 60 °C, the residual polymer was removed by RIE. The processing gases were O_2 (20 sccm), the RF power was 30 W, and the chamber pressure was 10 mTorr. After etching for 90 s, the patterned ITO was obtained.

ECD of AuNPs. A solution composed of $HAuCl_4$ (24.3 m mol/L) without any other supporting materials was used as the electrolyte. The patterned ITO was used as working electrode and clean ITO slice was used as counter electrode for the ECD process.[26] The ECD process was carried out on the BAS100W Electrochemical Analyzer (Bioanalytical Systems, West Lafayette, IN). After the ECD process, the resist polymer was removed by rinsing the substrate in acetone, followed by drying under a flow of pure nitrogen. Periodic gold particle arrays were fabricated on the ITO substrate by a single ECD process.

Characterization. Atomic force microscopy (AFM) measurements were taken on a Multimode Nanoscope IIIa instrument (Digital Instrument, Santa Barbara, CA), operated in the tapping mode with silicon cantilevers with a resonant frequency 280−340 kHz. The aspect ratio of AFM tip is 10 nm. Scanning electron microscope (SEM) images were collected on an environmental scanning electron microscope (ESEM, Model XL 30 ESEM FEG from Micro FEI Philips). The samples were sputtered with a thin layer of Au (2 nm in thickness) prior to imaging. X-ray diffraction (XRD) pattern was recorded on a Rigaku D/MAX 2500/PC X-ray diffractometer with graphite-filtered Cu Kα radiation, at 50 kV and 200 mA over the range 20−80° at a scanning rate of 10°/min.

RESULTS AND DISCUSSION

The fabrication process is schematically shown in Figure 1. The thermoplastic resist polymer (Mr-I 7030E) was spin-coated onto the substrate first, which was subsequently patterned with NIL. The stamp is of 500 nm in depth with periodicity of 580 nm, as shown in panels a and b in Figure 2. The height of the printed polymer structure is 490 nm, as shown in panels c and d in Figure 2. After conducting RIE, the ITO substrate was selectively exposed to air. The section analysis along the black line (Figure 2e) is conducted and the result is presented in Figure 2f. The diameter of the exposed area is 150 nm and the height of the structure is 460 nm on the patterned substrate. The ECD process was performed by using the patterned ITO substrate as working electrode to generate the gold particle arrays. The SEM image shows that the AuNPs are formed on the predefined area after ECD process (Figure 3a, b). The AuNPs are arranged hexagonally with the periodicity of 580 nm, corresponding to the size of original PS spheres. No particles can be observed along the walls of the pores because Au cannot nucleate on the insulating polymer. After lift-off

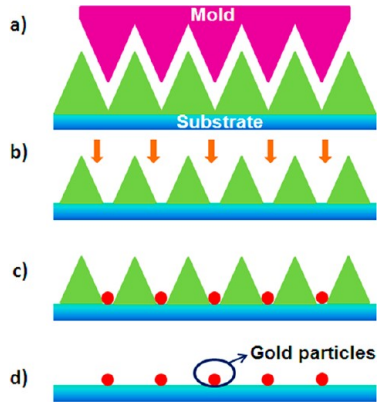

Figure 1. Schematic illustration of the procedures for fabricating the arrays of gold particles. (a) Patterning the spin-coated polymer film using NIL; (b) RIE process; (c) ECD of gold particles; (d) "lift-off" of the resist layer.

process, the arrays of the AuNPs can be obtained on the ITO substrates (Figure 3c). Figure 3d indicates that the AuNPs arrays can be extended to a large area. The hexagonal arrangement of the NPs is confirmed by the SEM image and its fast Fourier transform (FFT) image shown in the inset of Figure 3d. Figure S1 in the Supporting Information shows the typical XRD pattern of AuNPs arrays, which reveals that the as-prepared array is gold crystal with face-centered-cubic lattice structure.[37]

The size of the particle should depend on the nucleation rate and duration. According to the theory of crystallization, nucleation rate of Au grains is exponentially related to the driving force of electrocrystallization (overpotential). The size of the particle increases more rapidly when the applied voltage is higher, which is consistent with the nucleation theory.[38] According to the Tafel law

$$\eta = a + blgi \tag{1}$$

where η is overpotential, a and b are constants, and i is current density. Equation 1 reveals the higher current density leads to the higher overpotential. According to the nucleation rate formula[38]

$$J = N_0 \Gamma \omega_{a,c} \exp\left(\frac{-bs\varepsilon^2}{zek_B T\eta}\right) \tag{2}$$

where J is nucleation rate, N_0 and Γ are the number of adsorption sites and the Zeldovich factor, respectively, and $\omega_{a,c}$ is the attachment frequency of single atoms to the critical cluster; b is the geometric index; s is the area occupied by one atom on the surface of the nucleus; ε is the boundary energy; k_B is Boltzmann constant; e is elementary charge; z is ionic charge; T is the absolute temperature; and η is overpotential. Equation 2 reveals the nucleation rate J increases exponentially with increasing the overpotential η. From eqs 1 and 2, it can be concluded that higher current density leads to the higher nucleation rate.

To adjust the diameters of the AuNPs, ECD was carried out under different potentials with the same duration of 200 s. Under the potential of −100 mV, fewer nuclei are formed because of the low current density, as shown in Figure S2a in the Supporting Information. When the potential ranges from −100 to −200 mV, nucleation rate becomes higher as a result of the increased overpotential which is caused by the increased

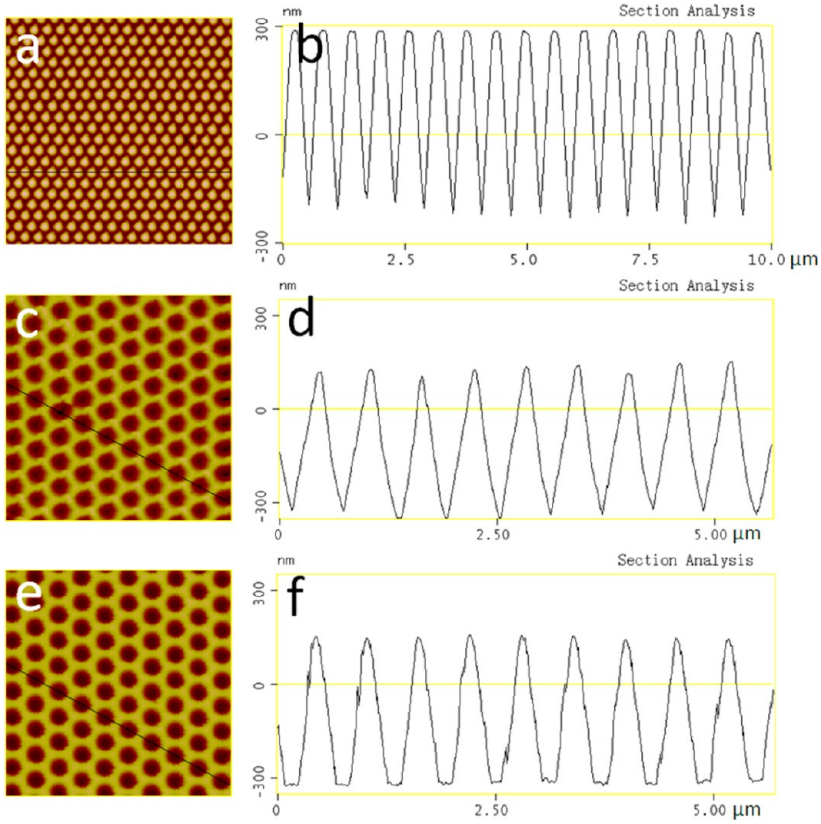

Figure 2. AFM images and the section analyses: (a, b) the stamp, with the depth of 500 nm; (c, d) polymer resist pattern after normal NIL process, with the height of 490 nm; (e, f) polymer resist pattern after RIE for 90 s, with the height of 460 nm and diameter of area exposed to air: 150 nm. The unit of the section analysis is μm in width and nm in height.

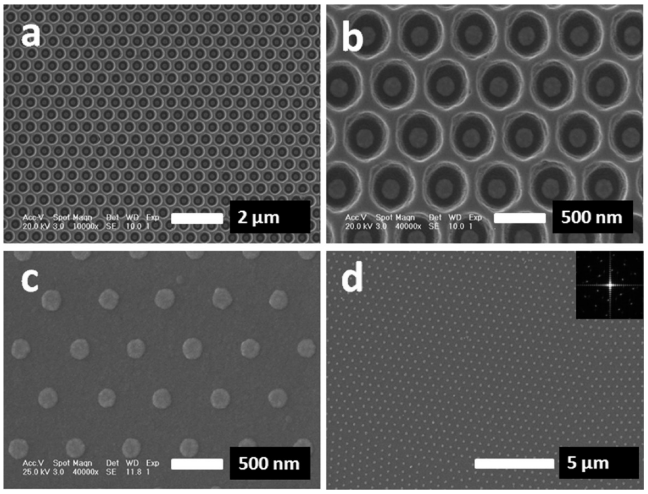

Figure 3. SEM images of (a) Au particle array before lift-off process and (b) a local magnification of a; (c) Au particle array after lift-off process; (d) Au particle array extend to a large area, and inset in the right display the corresponding FFT image. The scale bars a–d are 2 μm, 500 nm, 500 nm, and 5 μm, respectively.

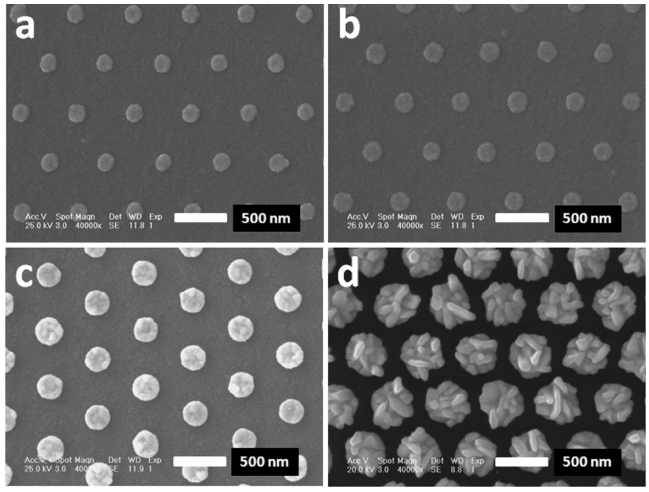

Figure 4. SEM images of gold particles under different potentials: (a) −300, (b) −400, (c) −500, and (d) −600 mV. All the samples were fabricated under the same duration 200 s. The scale bars are 500 nm.

current density i. With the same duration, the amount of nuclei at −200 mV is larger than that at −100 mV (see Figure S2b in the Supporting Information). As shown in Figure 4a, with the potential of −300 mV, the nucleation rate increases exponentially with increasing overpotential, thus more AuNPs were deposited, and the spacing between the AuNPs disappeared, the nucleus form a spherical gold particle as a result of size confinement. When the potential ranges from −300 mV to −600 mV, nucleation rate increases exponentially, and the size of gold particles increases. The size of AuNPs can be adjusted by varying the potential. When the size of the AuNPs is increased with increasing the ECD potential, the gap between the particles becomes smaller because the period of the pattern is constant. As shown in Figure 4a–d, the diameter of the particles ranges from 167 to 420 nm when potential ranges from −300 mV to −600 mV. Correspondingly, the

dx.doi.org/10.1021/am3010972 | ACS Appl. Mater. Interfaces 2012, 4, 3779–3783

height of particles ranges from 35 to 170 nm (see Figure S3 in the Supporting Information). The overall volume of the nanoparticle increases as a result of the increased nucleation rate when potential ranges from −300 to −600 mV. Specially, the morphology changes seriously when the potential is set to −500 and −600 mV. In this case, growth instabilities can lead to preferential attachment of metal ions at protuberances resulting in the formation of unusual morphologies.[39] However, when the potential is −700 mV, large irregular particles overgrow out of the holes (see Figure S4 in the Supporting Information).

The sizes of AuNPs also can be tuned by varying the ECD duration from 30 to 1100 s. Figure 5 shows the AuNPs arrays

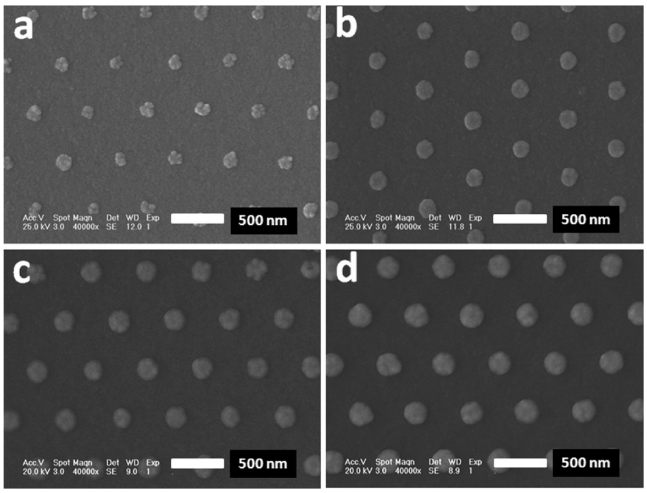

Figure 5. SEM images of gold particles under different durations: (a) 60 s, (b) 200 s, (c) 500 s, and (d) 1100 s. All the samples were under the same potential −300 mV. The scale bars are 500 nm.

obtained by taking different duration of ECD at the same potential of −300 mV. When the duration was 30 s, only a few small grains formed because the amount of deposited gold was not big enough to form a spherical particle and grains were easily washed away during lift-off process as a result of small contact area with ITO substrate (see Figure S5a, b in the Supporting Information). Upon increasing the deposition duration, the gold particle size increased because more gold deposited. As shown in Figure 5a, with extending the duration to 60 s, a small particle formed and the spacing between the Au grains disappeared. As revealed in Figure 5b−d, the diameter of the AuNPs changes from 130 to 237 nm by further increasing the duration. AFM studies of the height of these structures are shown in Figure S6 in the Supporting Information. The height of the AuNPs increases slowly from 30 to 43 nm when duration ranges from 60 to 1100 s.

The correlation of the particle diameter and the value of potential is shown in Figure 6a. The particle diameter increases with increasing potential. The variation of the slope reveals the nucleation rate increases exponentially with increasing potential. The correlation of the particle diameter and duration is shown in Figure 6b. The particle size increases with prolonging the duration. The variation in the slope reveals that the increased speed of the particle size becomes smaller because the concentration of gold ion in the vicinity of the cathode decreases, and therefore the process would become diffusion-controlled.

CONCLUSIONS

In conclusion, we demonstrated a method to fabricate an ordered Au particle array based on NIL and ECD. The stamp for NIL was fabricated by NSL, which is cost-efficient. The size of the particles can be easily controlled by adjusting the potential and duration of ECD using the same stamp. In this work, the diameters of AuNPs are varied from 130 to 420 nm. Furthermore, this method may have potential applications in fabricating AuNP arrays with different periodicities by applying PS spheres with different sizes. The AuNP arrays can be readily extended to other conductive substrates, which may be applied for detecting and sensing.

ASSOCIATED CONTENT

Supporting Information

XRD patterns of AuNP arrays, SEM images of gold particles under low potentials, AFM images and the section analyses of AuNPs under different potentials, SEM images of Au particles under ECD potential −700 mV and duration of 200 s, SEM images of AuNPs under ECD potential −300 mV and duration of 30 s, AFM images and the section analyses of AuNPs under different durations. This material is available free of charge via the Internet at http://pubs.acs.org/.

AUTHOR INFORMATION

Corresponding Author

*E-mail: luenan@jlu.edu.cn. Tel/Fax: +86-431-85168477.

Notes

The authors declare no competing financial interest.

ACKNOWLEDGMENTS

The authors gratefully acknowledge Xu Liu for her assistance on the XRD characterization. This work was supported by the

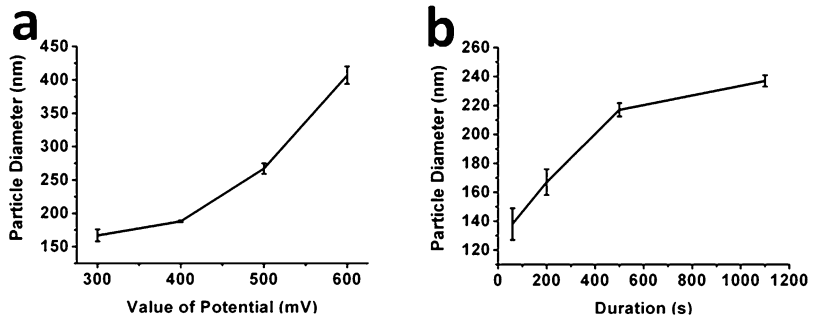

Figure 6. Correlation of particle diameter and (a) value of ECD potential, (b) ECD duration.

National Basic Research Program (2007CB808003, 2009CB939701).

REFERENCES

(1) Chen, S.; Svedendahl, M.; Duyne, R. P.; Kall, M. *Nano Lett.* **2011**, *11*, 1826−1830.
(2) Mayer, K. M.; Hafner, J. H. *Chem. Rev.* **2011**, *111*, 3828−3857.
(3) Kuznetsov, A. I.; Evlyukhin, A. B.; Goncalves, M. R.; Reinhardt, C.; Koroleva, A.; Arnedillo, M. L.; Kiyan, R.; Marti, O.; Chichkov, B. N. *ACS Nano* **2011**, *5*, 4843−4849.
(4) Komanicky, V.; Iddir, H.; Chang, K. C.; Menzel, A.; Karapetrov, G.; Hennessy, D.; Zapol, P.; You, H. *J. Am. Chem. Soc.* **2009**, *131*, 5732−5733.
(5) Hong, A. J.; Liu, C. C.; Wang, Y.; Kim, J.; Xiu, F.; Ji, S.; Zou, J.; Nealey, P. F.; Wang, K. L. *Nano Lett.* **2010**, *10*, 224−229.
(6) Huang, Z. P.; Fang, H.; Zhu, J. *Adv. Mater.* **2007**, *19*, 744−748.
(7) Huang, J. Q.; Chiam, S. Y.; Tan, H. H.; Wang, S. J.; Chim, W. K. *Chem. Mater.* **2010**, *22*, 4111−4116.
(8) Chen, J. K.; Qui, J. Q.; Fan, S. K.; Kuo, S. W.; Ko, F. H.; Chu, C. W.; Chang, F. C. *J. Colloid Interface Sci.* **2012**, *367*, 40−48.
(9) Kempa, K.; Kimball, B.; Rybczynski, J.; Huang, Z. P.; Wu, P. F.; Steeves, D.; Sennett, M.; Giersig, M.; Rao, D. V. G. L. N.; Carnahan, D. L.; Wang, D. Z.; Lao, J. Y.; Li, W. Z.; Ren, Z. F. *Nano Lett.* **2003**, *3*, 13−18.
(10) Liu, D. F.; Xiang, Y. J.; Wu, X. C.; Zhang, Z. X.; Liu, L. F.; Song, L.; Zhao, X. W.; Luo, S. D.; Ma, W. J.; Shen, J.; Zhou, W. Y.; Wang, G.; Wang, C. Y.; Xie, S. S. *Nano Lett.* **2006**, *6*, 2375−2378.
(11) Liu, D. F.; Xiang, Y. J.; Liao, Q.; Zhang, J. P.; Wu, X. C.; Zhang, Z. X.; Liu, L. F.; Ma, W. J.; Shen, J.; Zhou, W. Y.; Xie, S. S. *Nanotechnology* **2007**, *18*, 405303.
(12) Fan, S. S.; Chapline, M. G.; Franklin, N. R.; Tombler, T. W.; Cassell, A. M.; Dai, H. J. *Science* **1999**, *283*, 512−514.
(13) Huang, M. H.; Mao, S.; Feick, H.; Yan, H.; Wu, Y.; Kind, H.; Weber, E.; Russo, R.; Yang, P. *Science* **2001**, *292*, 1897−1899.
(14) Jain, P. K.; Huang, W. Y.; El-Sayed, M. A. *Nano Lett.* **2007**, *7*, 2080−2088.
(15) Ye, J.; Wen, F.; Sobhani, H.; Lassiter, J. B.; Dorpe, P. V.; Nordlander, P.; Halas, N. J. *Nano Lett.* **2012**, *12*, 1660−1667.
(16) Garno, J. C.; Zangmeister, C. D.; Batteas, J. D. *Langmuir* **2007**, *23*, 7874−7879.
(17) Xue, M.; Zhang, Z.; Zhu, N.; Wang, F.; Zhao, X. S.; Cao, T. *Langmuir* **2009**, *25*, 4347−4351.
(18) Jiang, L.; Wang, W.; Fuchs, H.; Chi, L. *Small* **2009**, *5*, 2819−2822.
(19) Choi, J. H.; Adams, S. M.; Ragan, R. *Nanotechnology* **2009**, *20*, 065301.
(20) Park, S.; Kim, B.; Wang, J. Y.; Russell, T. P. *Adv. Mater.* **2008**, *20*, 681−685.
(21) Mistark, P. A.; Park, S.; Yalcin, S. E.; Lee, D. H.; Yavuzcetin, O.; Tuominen, M. T.; Russell, T. P.; Achermann, M. *ACS Nano* **2009**, *3*, 3987−3992.
(22) Kim, S. H.; Misner, M. J.; Xu, T.; Kimura, M.; Russell, T. P. *Adv. Mater.* **2004**, *16*, 226−231.
(23) Mu, C.; Zhang, J.-P.; Xu, D. *Nanotechnology* **2010**, *21*, 015604.
(24) Choi, D.; Choi, Y.; Hong, S.; Kang, T.; Lee, L. P. *Small* **2010**, *6*, 1741−1744.
(25) Yang, S.; Lei, Y. *Nanoscale* **2011**, *3*, 2768−2782.
(26) Yang, B.; Lu, N.; Huang, C.; Qi, D.; Shi, G.; Xu, H.; Chen, X.; Dong, B.; Song, W.; Zhao, B.; Chi, L. *Langmuir* **2009**, *25*, 55−58.
(27) Luo, L.-B.; Chen, L.-M.; Zhang, M.-L.; He, Z.-B.; Zhang, W.-F.; Yuan, G.-D.; Zhang, W.-J.; Lee, S.-T. *J. Phys. Chem. C* **2009**, *113*, 9191−9196.
(28) Sun, F.; Cai, W.; Li, Y.; Cao, B.; Lu, F.; Duan, G.; Zhang, L. *Adv. Mater.* **2004**, *16*, 1116−1121.
(29) Krishnamoorthy, S.; Krishnan, S.; Thoniyot, P.; Low, H. Y. *ACS Appl. Mater. Interfaces* **2011**, *3*, 1033−1040.
(30) Kuo, C.-W.; Shiu, J.-Y.; Cho, Y.-H.; Chen, P. *Adv. Mater.* **2003**, *15*, 1065−1068.
(31) Kuo, C.-W.; Shiu, J.-Y.; Cho, Y.-H.; Chen, P. *Chem. Mater.* **2003**, *15*, 2917−2920.
(32) Li, W.; Xu, L.; Zhao, W.-M.; Sun, P.; Huang, X.-F.; Chen, K.-J. *Appl. Surf. Sci.* **2007**, *253*, 9035−9038.
(33) Zhou, W.; Zhang, J.; Li, X.; Liu, Y.; Min, G.; Song, Z.; Zhang, J. *Appl. Surf. Sci.* **2009**, *255*, 8019−8022.
(34) Lee, P.-S.; Lee, O.-J.; Hwang, S.-K.; Jung, S.-H.; Jee, S. E.; Lee, K.-H. *Chem. Mater.* **2005**, *17*, 6181−6185.
(35) Park, H. J.; Kang, M.-G.; Guo, L. J. *ACS Nano* **2009**, *3*, 2601−2608.
(36) Xu, H.; Lu, N.; Qi, D.; Hao, J.; Gao, L.; Zhang, B.; Chi, L. *Small* **2008**, *4*, 1972−1975.
(37) Sun, Y.; Xia, Y. *Science* **2002**, *298*, 2176−2179.
(38) Budevski, E.; Bostanov, V.; Staikov, G. *Annu. Rev. Mater. Sci.* **1980**, *10*, 85−112.
(39) Guo, L.; Searson, P. C. *Electrochim. Acta* **2010**, *55*, 4086−4091.